A SIMPLIFIED TIRE MODEL BASED ON A ROTATING SHELL

N. Alujević[1], N. Campillo-Davo[2], P. Kindt[3], W. Desmet[1], B. Pluymers[1], S. Vercammen[3]
[1] KU Leuven,
Production Engineering, Machine Design and Automation (PMA) Section
Celestijnenlaan 300b - box 2420
3001 Heverlee,
Belgium
email: neven.alujevic@mech.kuleuven.be

[2] Universidad Miguel Hernandez de Elche,
Dpto. de Ingeniería Mecánica y Energía. Área de Ingeniería Mecánica.
Avda. de la Universidad, s/n. Edif. Quorum V
03202 - Elche (Alicante),
Spain

[3] Goodyear S.A.
Innovation Center,
L-7750 Colmar-Berg,
Luxembourg

A number of simplified models of rotating tires have been suggested in the past. The belt had been modelled as a cylindrical shell, almost exclusively having simply supported boundary conditions. Such models are unable to represent certain groups of mode shapes due to the assumed zero radial displacements at the ends of the tire belt. In this paper, a model using free boundary conditions is reported. The developed model is able to approximate mode shapes that are similar to Rayleigh and Love symmetric and anti-symmetric mode shapes. Mode shapes, natural frequencies and their veering with rotation speed are calculated exactly.

1 INTRODUCTION

The effects of rotation significantly alter the dynamic behaviour of automotive tires [1]. In non-rotating tires, vibrations are characterized by pairs of traveling modes that rotate in opposite directions but have the same speed of rotation. The travelling modes thus superimpose, which results in formation of a stationary (non-rotating) vibration mode. On the contrary, if the tire rotates, the two modes rotate with different speeds [2]. This is due to the Coriolis effects which alter the propagation speed of the two otherwise superimposing modes in the co-rotating reference frame. Also the Doppler Effect plays a role when observing the vibrations from a fixed reference frame.

A great number of studies have been concerned with analysis of the effects of rotation onto vibrations of rotating tires. For example, in order to capture detailed dynamics of a rotating tire, complex numerical models have been developed accounting for non-homogenous structural properties of the tire belt and sidewall, structural-acoustic coupling and complex geometry description (including that of the wheel rim), under varying rotation speeds [3]. However, although a remarkable amount of details can be successfully modelled using such an approach, it can be rather difficult to parameterize the model, i.e. to establish clear-cut relationships between geometrical or material properties of the tire and the corresponding influence onto the tire dynamics.

An alternative way of studying vibration of rotating tires is to utilise simplified, analytical models using the theory of cylindrical shells [2], [4-6]. The principal assumption used in such tire models is that the geometry of the tire belt can be simplified through a cylindrical shell approximation with homogeneous, smeared material properties. Additionally, the air and sidewall stiffness are roughly approximated using an elastic foundation beneath the shell surface, which has distributed radial and circumferential stiffnesses. Also, the pressurisation and the centrifugal force can be approximately taken into account via an initial circumferential tension (hoop stress) in the belt.

However, closed form solutions for resonance frequencies and mode shapes of shell-like structures are possible only for certain geometries and in combinations with mathematically convenient boundary conditions. If the effects of rotation are to be studied as well, then it becomes even more difficult to

derive the closed form expressions. For example, Huang and Soedel [4] used the strain-displacement relationships of Herrmann and Armenakas [6], and solved the free and forced vibration problem assuming simply supported boundary conditions. The natural frequencies were calculated as roots of a characteristic polynomial, which was shown to be bi-cubic if the shell does not rotate, or of full order of six if the shell rotates around the axis of symmetry.

A drawback of such models assuming the simply supported boundary conditions is that they are unable to represent certain groups of mode shapes that occur with real tires. This is due to the assumed zero radial displacements at the ends of the tire belt. This would be an unnecessary constraint of the infinite radial stiffness of the sidewall.

In this study, a model for rotating cylindrical shells with free boundary conditions is developed. This is thought to be a more useful set of boundary conditions if the shell is to be used for modelling a tire belt. This is because the present model is able to approximate also mode shapes that are similar to the so-called Rayleigh and Love symmetric and anti-symmetric mode shapes.

The drawback of the present model, however, is that the calculation of the mode shapes and resonance frequencies is rather complex because it is done in a fully analytical manner (the free vibration problem is solved exactly). Nevertheless, once developed, the model allows for calculating the resonance frequencies and the mode shapes of the rotating shell as a function of some basic geometrical and material properties as well as the rotation speed. The paper is structured as follows. The mathematical model is briefly presented in the first section, and an example shell is considered in the second section, which is followed by a conclusions section.

2 MATHEMATICAL MODEL

The rotating cylindrical shell is shown schematically in *Figure 1 (a)*.

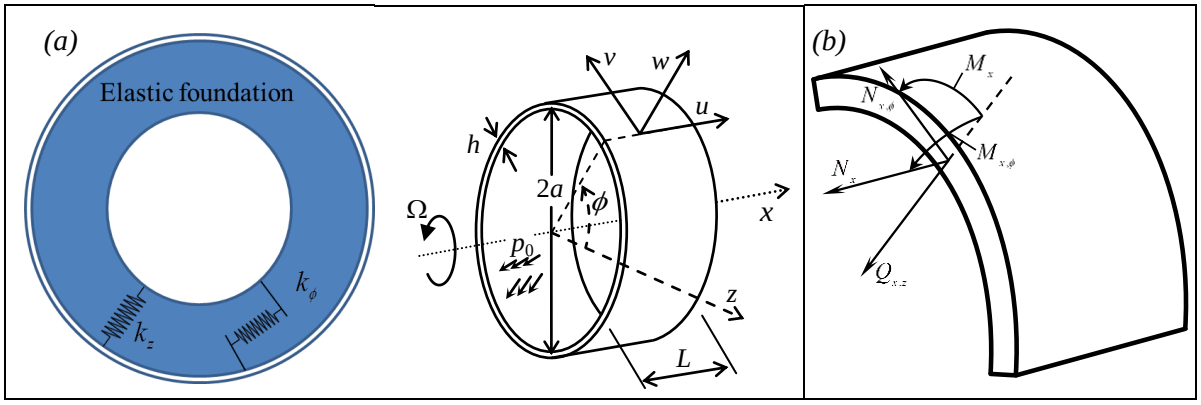

Figure 1: (a) The scheme of a rotating cylindrical shell, and (b) the shell boundary force resultants

The equations of motions, assuming the free vibration problem, are [4]:

$$\begin{bmatrix} \mathcal{L}_{x,u}+\rho h\frac{\partial^2}{\partial t^2} & \mathcal{L}_{x,v} & \mathcal{L}_{x,w} \\ \mathcal{L}_{\phi,u} & \mathcal{L}_{\phi,v}+\rho h(\frac{\partial^2}{\partial t^2}-\Omega^2) & \mathcal{L}_{\phi,w}+2\rho h\Omega\frac{\partial}{\partial t} \\ \mathcal{L}_{z,u} & \mathcal{L}_{z,v}-2\rho h\Omega\frac{\partial}{\partial t} & \mathcal{L}_{z,w}+\rho h(\frac{\partial^2}{\partial t^2}-\Omega^2) \end{bmatrix} \begin{Bmatrix} u \\ v \\ w \end{Bmatrix} = \mathbf{0}\,. \tag{1}$$

The linear operators $\mathcal{L}_{x,u}, \mathcal{L}_{x,v}, \mathcal{L}_{x,w}, \mathcal{L}_{\phi,u}, \mathcal{L}_{\phi,v}, \mathcal{L}_{\phi,w}$ and $\mathcal{L}_{z,u}, \mathcal{L}_{z,v}, \mathcal{L}_{z,w}$ are:

$$\mathcal{L}_{x,u}=\frac{(\mu-1)K-2N_{\phi,i}}{2a^2}\frac{d^2}{d\phi^2}-(K+N_{x,i})\frac{d^2}{dx^2}\,, \tag{2}$$

$$\mathscr{L}_{x,v} = -\frac{K(1+\mu)}{2a}\frac{d^2}{dxd\phi}, \tag{3}$$

$$\mathscr{L}_{x,w} = -\frac{\mu K}{a}\frac{d}{dx}, \tag{4}$$

$$\mathscr{L}_{\phi,u} = -\frac{K(1+\mu)}{2a}\frac{d^2}{dxd\phi}, \tag{5}$$

$$\mathscr{L}_{\phi,v} = \frac{(\mu-1)(Ka^2+D)-2N_{x,i}a^2}{2a^2}\frac{d^2}{dx^2} - \frac{\left(\left(K+N_{\phi,i}\right)a^2+D\right)}{a^4}\frac{d^2}{d\phi^2} + \frac{\left(k_\phi a^2+N_{\phi,i}\right)}{a^2}v, \tag{6}$$

$$\mathscr{L}_{\phi,w} = \frac{D}{a^4}\frac{d^3}{d\phi^3} - \frac{\left(K+2N_{\phi,i}\right)\frac{d}{d\phi} - D\frac{d^3}{dx^2d\phi}}{a^2}, \tag{7}$$

$$\mathscr{L}_{z,u} = \frac{\mu K}{a}\frac{d}{dx}, \tag{8}$$

$$\mathscr{L}_{z,v} = \frac{\left(K+2N_{\phi,i}\right)\frac{d}{d\phi} - D\frac{d^3}{dx^2d\phi}}{a^2} - \frac{D}{a^4}\frac{d^3}{d\phi^3}, \tag{9}$$

$$\mathscr{L}_{z,w} = \frac{D}{a^4}\frac{d^4}{d\phi^4} + \frac{D\left(2\frac{d^4}{dx^2d\phi^2}+a^2\frac{d^4}{dx^4}\right) - N_{\phi,i}\frac{d^2}{d\phi^2} - a^2N_{x,i}\frac{d^2}{dx^2} + \left(K+a^2k_z+N_{\phi,i}\right)}{a^2}, \tag{10}$$

where:

a	=	shell radius,
h	=	shell thickness,
L	=	shell length,
p_0	=	inflation pressure,
$u = u(x,\phi,t)$	=	axial displacement,
$v = v(x,\phi,t)$	=	tangential displacement,
$w = w(x,\phi,t)$	=	radial displacement,
x	=	axial coordinate,
ϕ	=	tangential coordinate,
z	=	radial coordinate,
μ	=	Poisson's ratio,
E	=	Young's modulus,
ρ	=	mass density,
k_ϕ	=	elastic foundation stiffness in the tangential direction,
k_z	=	elastic foundation stiffness in the radial direction,
$N_{x,i}$	=	initial tension in the axial direction,
$N_{\phi,i}$	=	initial tension in the tangential direction,
Ω	=	rotation speed,
$D = Eh^3/12(1-\mu^2)$	=	bending stiffness, and
$K = Eh/(1-\mu^2)$	=	membrane stiffness.

The initial tension in the tangential direction is given by [4]:

$$N_{\phi,i} = \rho h a^2\Omega^2 + ap_0, \tag{11}$$

where the first term is due to centrifugal forces and the second term is due to the initial inflation pressure of the shell. Substituting:

$$u = U_0 \mathrm{e}^{\frac{\alpha x}{a}} \cos\left(n\phi + \omega t\right), \tag{12}$$

$$v = V_0 \mathrm{e}^{\frac{\alpha x}{a}} \sin\left(n\phi + \omega t\right), \tag{13}$$

$$w = W_0 \mathrm{e}^{\frac{\alpha x}{a}} \cos\left(n\phi + \omega t\right), \tag{14}$$

into the equations of motion (1), yields:

$$\begin{bmatrix} k_{1,1,A} + k_{1,1,B}\alpha^2 & k_{1,2,B}\alpha & k_{1,3,B}\alpha \\ \textit{symm.} & k_{2,2,A} + k_{2,2,B}\alpha^2 & k_{2,3,A} + k_{2,3,B}\alpha^2 \\ \textit{symm.} & \textit{symm.} & k_{3,3,A} + k_{3,3,B}\alpha^2 + k_{3,3,C}\alpha^4 \end{bmatrix} \begin{Bmatrix} U_0 \\ V_0 \\ W_0 \end{Bmatrix} = \mathbf{0}, \tag{15}$$

where $k_{i,j,\sim}$ can be found in [7]. The determinant of the matrix in Eq. (15) must vanish in order for the equations of motion to be satisfied. Setting the determinant to zero yields the biquartic polynomial in α:

$$A_8\alpha^8 + A_6\alpha^6 + A_4\alpha^4 + A_2\alpha^2 + A_0 = 0, \tag{16}$$

where the coefficients A_r in function of $k_{i,j,\sim}$ are given in [7]. So there are eight roots of the polynomial and so the radial component of the displacement can be expressed as:

$$w = W(x)\cos\left(n\phi + \omega t\right), \tag{17}$$

with:

$$W(x) = \sum_{r=1}^{8} B_r e^{\frac{\alpha_r x}{a}}, \tag{18}$$

where B_r, with r=1…8, are eight generally complex constants. The roots of the polynomial (16) may be calculated at this stage by assuming the frequency ω.

The roots can take eight types of forms as listed in *Table 1* below.

Table 1 The eight types or roots of the characteristic bi-quartic polynomial

Case	1	2	3	4	5	6	7	8
Roots	$\pm\alpha_1$, $\pm\mathrm{i}\gamma_2$, $\pm(p \pm \mathrm{i}q)$	$\pm(f \pm \mathrm{i}g)$, $\pm(p \pm \mathrm{i}q)$	$\pm\alpha_1$, $\pm\alpha_2$, $\pm(p \pm \mathrm{i}q)$	$\pm\alpha_1$, $\pm\alpha_2$, $\pm\alpha_3$, $\pm\alpha_4$	$\pm\alpha_1$, $\pm\alpha_2$, $\pm\alpha_3$, $\pm\mathrm{i}\gamma_4$	$\pm\alpha_1$, $\pm\alpha_2$, $\pm\mathrm{i}\gamma_3$, $\pm\mathrm{i}\gamma_4$	$\pm\alpha_1$, $\pm\mathrm{i}\gamma_2$, $\pm\mathrm{i}\gamma_3$, $\pm\mathrm{i}\gamma_4$	$\pm\mathrm{i}\gamma_1$, $\pm\mathrm{i}\gamma_2$, $\pm(p \pm \mathrm{i}q)$

The complete set of solutions for all roots can be found in [7]. Here only the first type of roots (Case 1 in *Table 1*) is covered for brevity. Note that α_1, γ_2, p, q are real and positive numbers. In such a case the radial component of the displacement is given by:

$$\begin{aligned} W(x) = {} & C_1 \cosh\left(\frac{\alpha_1 x}{a}\right) + C_2 \sinh\left(\frac{\alpha_1 x}{a}\right) + C_3 \cos\left(\frac{\gamma_2 x}{a}\right) + C_4 \sin\left(\frac{\gamma_2 x}{a}\right) + \\ & + e^{\frac{px}{a}}\left(C_5 \cos\left(\frac{qx}{a}\right) + C_6 \sin\left(\frac{qx}{a}\right)\right) + e^{\frac{-px}{a}}\left(C_7 \cos\left(\frac{qx}{a}\right) + C_8 \sin\left(\frac{qx}{a}\right)\right) \end{aligned}, \tag{19}$$

where C_r are now real constants.

From Eq. (15):

$$\left(\frac{U}{W}\right)_r = \frac{k_{1,2}k_{2,3} - k_{1,3}k_{2,2}}{k_{1,1}k_{2,2} - k_{1,2}^2}, \tag{20}$$

and

$$\left(\frac{V}{W}\right)_r = \frac{k_{1,2}k_{1,3} - k_{2,3}k_{1,1}}{k_{1,1}k_{2,2} - k_{1,2}^2}, \tag{21}$$

where $k_{1,1} = k_{1,1,A} + k_{1,1,B}\alpha^2$, $k_{1,2} = k_{1,2,B}\alpha$, $k_{1,3} = k_{1,3,B}\alpha$, $k_{2,2} = k_{2,2,A} + k_{2,2,B}\alpha^2$, $k_{2,3} = k_{2,3,A} + k_{2,3,B}\alpha^2$. Substituting for each root α_r into Eqs. (20) and (21), the expressions for $U(x)$ and $V(x)$ can be represented as:

$$\begin{aligned} V(x) &= d_1C_1\cosh\left(\frac{\alpha_1 x}{a}\right) + d_1C_2\sinh\left(\frac{\alpha_1 x}{a}\right) + d_3C_3\cos\left(\frac{\gamma_2 x}{a}\right) + d_3C_4\sin\left(\frac{\gamma_2 x}{a}\right) + \\ &+ e^{\frac{px}{a}}\left(\left(d_5C_5 + d_6C_6\right)\cos\left(\frac{qx}{a}\right) + \left(d_5C_6 - d_6C_5\right)\sin\left(\frac{qx}{a}\right)\right) + \\ &+ e^{\frac{-px}{a}}\left(\left(d_5C_7 - d_6C_8\right)\cos\left(\frac{qx}{a}\right) + \left(d_5C_8 + d_6C_7\right)\sin\left(\frac{qx}{a}\right)\right) \end{aligned}, \tag{22}$$

$$\begin{aligned} U(x) &= d_2C_2\cosh\left(\frac{\alpha_1 x}{a}\right) + d_2C_1\sinh\left(\frac{\alpha_1 x}{a}\right) + d_4C_4\cos\left(\frac{\gamma_2 x}{a}\right) - d_4C_3\sin\left(\frac{\gamma_2 x}{a}\right) + \\ &+ e^{\frac{px}{a}}\left(\left(d_7C_5 + d_8C_6\right)\cos\left(\frac{qx}{a}\right) + \left(d_7C_6 - d_8C_5\right)\sin\left(\frac{qx}{a}\right)\right) + \\ &+ e^{\frac{-px}{a}}\left(\left(-d_7C_7 + d_8C_8\right)\cos\left(\frac{qx}{a}\right) - \left(d_7C_8 + d_8C_7\right)\sin\left(\frac{qx}{a}\right)\right) \end{aligned}. \tag{23}$$

The constants d_r can now be calculated using Eqs. (20) and (21) as [8]: $d_1 = \left(V/W\right)_r$ with $\alpha_r = \alpha_1, d_2 = \left(U/W\right)_r$ with $\alpha_r = \alpha_1, d_3 = \left(V/W\right)_r$ with $\alpha_r = \mathrm{i}\gamma_2, d_4 = \Im\left(U/W\right)_r$ with $\alpha_r = \mathrm{i}\gamma_2, d_5 = \Re\left(V/W\right)_r$ with $\alpha_r = p + \mathrm{i}q, d_6 = \Im\left(V/W\right)_r$ with $\alpha_r = p + \mathrm{i}q, d_7 = \Re\left(U/W\right)_r$ with $\alpha_r = p + \mathrm{i}q, d_8 = \Im\left(U/W\right)_r$ with $\alpha_r = p + \mathrm{i}q$ .At each end of the shell marked with *x=const.* there are five resultant forces as shown in *Figure 1 (b)*. The equations of motion are however of maximum fourth order and can only accommodate for four boundary conditions [9-10]. Thus the Kirchhoff effective shear stress resultant of the first kind, V_{xz}, and the Kirchhoff effective shear stress resultant of the second kind, $T_{x\phi}$, must be used that relate $Q_{x,z}$ to $M_{x,\phi}$, and $N_{x,\phi}$ to $M_{x,\phi}$, respectively [9-10]. The relations are [10]:

$$V_{xz} = Q_{xz} + \frac{1}{a}\frac{\partial M_{x\phi}}{\partial \phi}, \tag{24}$$

and

$$T_{x\phi} = N_{x\phi} + \frac{1}{a}M_{x\phi}. \tag{25}$$

Thus, the four boundary conditions for a shell with both ends free are:

$$N_x = 0; \quad \Rightarrow \quad a\frac{\partial u}{\partial x} + \mu w + \mu\frac{\partial v}{\partial \phi} = 0, \tag{26}$$

$$M_x = 0; \quad \Rightarrow \quad a^2\frac{\partial^2 w}{\partial x^2} + \mu\left(\frac{\partial^2 w}{\partial \phi^2} - \frac{\partial v}{\partial \phi}\right) = 0, \tag{27}$$

$$V_{xz} = 0; \quad \Rightarrow \quad \left(2 - \mu\right)\frac{\partial^3 w}{\partial x \partial \phi^2} - \frac{\partial^2 v}{\partial x \partial \phi} + a^2\frac{\partial^3 w}{\partial x^3} = 0, \tag{28}$$

$$T_{x\phi} = 0; \quad \Rightarrow -2h^2 \frac{\partial^2 w}{\partial x \partial \phi} + \left(12a^2 + h^2\right)\frac{\partial v}{\partial x} + 12a\frac{\partial u}{\partial \phi} = 0\,. \tag{29}$$

Since the boundary conditions are the same at the two ends, the modes can be either symmetric or anti-symmetric, or in other words, they cannot be asymmetric. Consequently the boundary conditions can be separately satisfied for symmetric and anti-symmetric modes by assuming the origin in the middle section of the cylinder and the boundaries at $x = \pm L/2$. Here the radial and the circumferential displacement components share the symmetry or anti-symmetry properties. The axial displacement component mathematical symmetry or anti-symmetry is opposite to that of the radial and circumferential displacement components but the physical symmetry is also the same. In case the modes are symmetric, the radial component of the displacement can be shortened by using $e^{\pm px/a} = \cosh(px/a) \pm \sinh(px/a)$ and ensuring that the anti-symmetric terms in Eq. (19) vanish. Then it must be $C_2 = C_4 = 0,\ C_5 = C_7$, and $C_6 = -C_8$, so that Eqs. (19), (22) and (23) reduce to:

$$W(x) = C_1\cosh\left(\frac{\alpha_1 x}{a}\right) + C_3\cos\left(\frac{\gamma_2 x}{a}\right) + F_1\cosh\left(\frac{px}{a}\right)\cos\left(\frac{qx}{a}\right) + F_2\sinh\left(\frac{px}{a}\right)\sin\left(\frac{qx}{a}\right), \tag{30}$$

$$\begin{aligned} V(x) = {} & d_1 C_1\cosh\left(\frac{\alpha_1 x}{a}\right) + d_3 C_3\cos\left(\frac{\gamma_2 x}{a}\right) + \left(d_5 F_1 + d_6 F_2\right)\cosh\left(\frac{px}{a}\right)\cos\left(\frac{qx}{a}\right) + \\ & + \left(d_5 F_2 - d_6 F_1\right)\sinh\left(\frac{px}{a}\right)\sin\left(\frac{qx}{a}\right) \end{aligned}, \tag{31}$$

$$\begin{aligned} U(x) = {} & d_2 C_1\sinh\left(\frac{\alpha_1 x}{a}\right) - d_4 C_3\sin\left(\frac{\gamma_2 x}{a}\right) + \left(d_7 F_1 + d_8 F_2\right)\sinh\left(\frac{px}{a}\right)\cos\left(\frac{qx}{a}\right) + \\ & + \left(d_7 F_2 - d_8 F_1\right)\cosh\left(\frac{px}{a}\right)\sin\left(\frac{qx}{a}\right) \end{aligned}. \tag{32}$$

Substituting Eq. (30) into (17) for the radial displacement component, and also Eqs. (31) and (32) into analogue expressions for tangential and axial displacement components gives a set of displacement components *u*, *v* and *w*. These can be substituted into Eqs. (26)-(29), which after assuming $x = L/2$ and putting into a matrix form gives:

$$\begin{bmatrix} t_{1,1}\cosh(\theta_1) & t_{1,2}\cos(\theta_2) & \begin{matrix} t_{1,3,\mathrm{A}}\cos(\theta_4)\cosh(\theta_3) + \\ +t_{1,3,\mathrm{B}}\sin(\theta_4)\sinh(\theta_3) \end{matrix} & \begin{matrix} t_{1,4,\mathrm{A}}\cos(\theta_4)\cosh(\theta_3) + \\ +t_{1,4,\mathrm{B}}\sin(\theta_4)\sinh(\theta_3) \end{matrix} \\ t_{2,1}\cosh(\theta_1) & t_{2,2}\cos(\theta_2) & \begin{matrix} t_{2,3,\mathrm{A}}\cos(\theta_4)\cosh(\theta_3) + \\ +t_{2,3,\mathrm{B}}\sin(\theta_4)\sinh(\theta_3) \end{matrix} & \begin{matrix} t_{2,4,\mathrm{A}}\cos(\theta_4)\cosh(\theta_3) + \\ +t_{2,4,\mathrm{B}}\sin(\theta_4)\sinh(\theta_3) \end{matrix} \\ t_{3,1}\sinh(\theta_1) & t_{3,2}\sin(\theta_2) & \begin{matrix} t_{3,3,\mathrm{A}}\sin(\theta_4)\cosh(\theta_3) + \\ +t_{3,3,\mathrm{B}}\cos(\theta_4)\sinh(\theta_3) \end{matrix} & \begin{matrix} t_{3,4,\mathrm{A}}\sin(\theta_4)\cosh(\theta_3) + \\ +t_{3,4,\mathrm{B}}\cos(\theta_4)\sinh(\theta_3) \end{matrix} \\ t_{4,1}\sinh(\theta_1) & t_{4,2}\sin(\theta_2) & \begin{matrix} t_{4,3,\mathrm{A}}\sin(\theta_4)\cosh(\theta_3) + \\ +t_{4,3,\mathrm{B}}\cos(\theta_4)\sinh(\theta_3) \end{matrix} & \begin{matrix} t_{4,4,\mathrm{A}}\sin(\theta_4)\cosh(\theta_3) + \\ +t_{4,4,\mathrm{B}}\cos(\theta_4)\sinh(\theta_3) \end{matrix} \end{bmatrix} \begin{Bmatrix} C_1 \\ C_3 \\ F_1 \\ F_2 \end{Bmatrix} = 0\,, \tag{33}$$

where $\theta_1 = \frac{\alpha_1 L}{2a}$, $\theta_2 = \frac{\gamma_2 L}{2a}$, $\theta_3 = \frac{pL}{2a}$ and $\theta_4 = \frac{qL}{2a}$. The coefficients $t_{r,s,\sim}$ depend on the roots α_1, γ_2, p, q, the constants d_r, n and μ, and are listed in [7]. In order to satisfy the boundary conditions, the determinant of the matrix in Eq. (33) must vanish. The determinant, after being divided by $\sinh\left(\frac{pL}{2a}\right)\cdot\sinh\left(\frac{\alpha_1 L}{2a}\right)\cdot\cosh\left(\frac{pL}{2a}\right)$ for better numerical behaviour, is given by:

$$\begin{aligned}&\left(\left(\tanh(\theta_3)b_1b_2\cos(\theta_2)+\sin(\theta_2)b_3\right)\coth(\theta_1)+b_4\cos(\theta_2)-\sin(\theta_2)\coth(\theta_3)b_5b_6\right)\cos(\theta_4)^2+\\&+\left(\begin{matrix}\left(b_7b_2\cos(\theta_2)+\left(b_9\coth(\theta_3)+\tanh(\theta_3)b_8\right)\sin(\theta_2)\right)\coth(\theta_1)+\\+\left(b_{11}\coth(\theta_3)+b_{10}\tanh(\theta_3)\right)\cos(\theta_2)+\sin(\theta_2)b_5b_{12}\end{matrix}\right)\times\sin(\theta_4)\cos(\theta_4)+\\&+\left(\left(\coth(\theta_3)b_{13}b_2\cos(\theta_2)+b_{14}\sin(\theta_2)\right)\coth(\theta_1)+b_{15}\cos(\theta_2)+\sin(\theta_2)\tanh(\theta_3)b_5b_{16}\right)\sin(\theta_4)^2=0\end{aligned}, \quad (34)$$

where coefficients b_r depending on $t_{r,s,\sim}$ are given in [7]. The zeroes of the left hand side of Eq. (34) in fact represent the length of the shell whose *m,n* mode resonates at the assumed frequency $\omega_{m,n}$, where the lowest zero (the smallest length) is for *m*=1 symmetric mode, the next one is for *m*=3 symmetric mode etc. According to this notation there are *m*+1 axial nodes (the cross-sections where *w*=0) for a mode number *m*. In case of a non-rotating shell ($\Omega = 0$), assuming frequencies $\pm|\omega_{m,n}|$ yields the same length for either the positive or the negative frequency $\omega_{m,n}$. However for $\Omega \neq 0$ this is not the case, since the forward and backward rotating modes are now characterised by different rotation speeds. Thus for rotating shells negative frequencies must be assumed in order to account for the forward rotating modes.

In case of anti-symmetric modes it must be $C_1 = C_3 = 0$, $C_5 = -C_7$, and $C_6 = C_8$ so that:

$$W(x) = C_2 \sinh\left(\frac{\alpha_1 x}{a}\right) + C_4 \sin\left(\frac{\gamma_2 x}{a}\right) + F_3 \sinh\left(\frac{px}{a}\right)\cos\left(\frac{qx}{a}\right) + F_4 \cosh\left(\frac{px}{a}\right)\sin\left(\frac{qx}{a}\right), \quad (35)$$

with similar expressions for $V(x)$ and $U(x)$. After recalculating the determinant for the anti-symmetric modes an expression analogue to Eq. (34) results, which can be obtained by substituting $\tanh(\theta_1) \rightleftarrows \coth(\theta_1)$, $\tanh(\theta_3) \rightleftarrows \coth(\theta_3)$, $\cos(\theta_2) \rightarrow \sin(\theta_2)$, and $\sin(\theta_2) \rightarrow -\cos(\theta_2)$ into Eq. (34). Then the zeroes represent the length of the shell whose *m,n* mode resonates at the assumed frequency $\omega_{m,n}$, where the lowest zero is for *m*=0 anti-symmetric mode (Love-type mode with one nodal cross section), the next one is for *m*=2 anti-symmetric mode etc. In order to calculate resonance frequencies for a shell of given length it is necessary to iterate until the length resulting from finding a zero of the determinant (34) matches the desired length of the shell to an acceptable precision. An alternative approach is also possible which utilises a detection of two frequencies between which the determinant (34) changes sign for the shell of a given length. In the following section an example rotating shell is considered and a number of mode shapes and resonance frequencies are calculated.

3 RESULTS

The example shell material and geometrical properties are listed in *Table 2*.

Table 2 The geometrical and material properties of the example shell

a (m)	h (m)	L (m)	ν (-)	ρ kgm^{-3}	E (GPa)	k_z (Nm^{-3})	k_ϕ (Nm^{-3})	p_0 (Pa)	$N_{x,i}$ (Nm^{-1})
0.1	0.002	0.2	0.45	1452	0.45	0	0	0	0

Figure 2 shows the resonance frequencies calculated using the methodology described above for the example shell as a function of the circumferential mode number up to 1 kHz (left plot) and from 1 kHz to 3kHz (right plot). The method for calculation of the resonance frequencies is as follows. The frequency range of interest (0-3 kHz) was divided into 30000 frequencies with an equidistant spacing of 0.1 Hz. Then a "scan" was performed through all frequencies in the range and a change in the sign of any of the sixteen determinants was detected between two adjacent frequencies assuming the shell length as in *Table 2*. The change of sign in fact indicates the existence of a mode with its resonance frequency between the two adjacent frequencies. Thus the accuracy of the calculated resonance frequencies is 0.1 Hz or better. As shown by the black continuous lines, it is in principle possible to calculate fictive resonance frequencies also for circumferential mode numbers which are not integers.

This has no physical meaning in the present study; however it enables to visually identify the so-called branches.

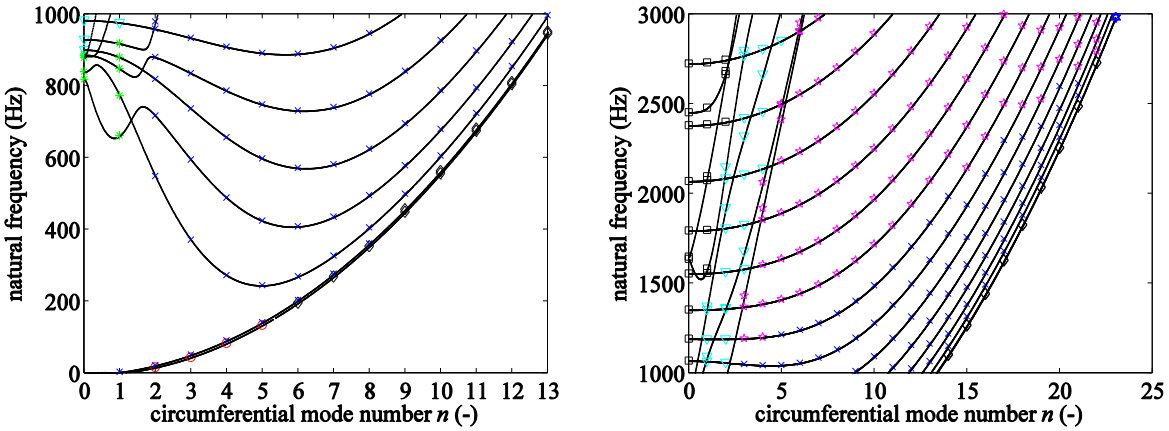

Figure 2: The natural frequencies of a stationary shell as a function of the circumferential mode number n; 0-1000 Hz (left) and 1000-3000 Hz (right). The root type is indicated by using different marker types: blue × mark – type 1, red circle – type 2, black diamond – type 3, blue hexagon – type 4, magenta pentagon – type 5, cyan triangle - type 6, black square – type 7, and finally, green asterisk – type 8, according to the notation given in Table 1.

Each branch contains resonance frequencies of modes having a constant axial mode number *m*. For example, the two branches with lowest resonance frequencies per a circumferential mode number contain the Rayleigh type (*m*=-1) and Love type modes (*m*=0), [8]. As can be seen in the plot these two groups of modes are characterised by very similar resonance frequencies, since the two branches nearly overlap. A depiction of a Love and a Rayleigh mode shape is given in *Figure 3*.

(a) *(b)*

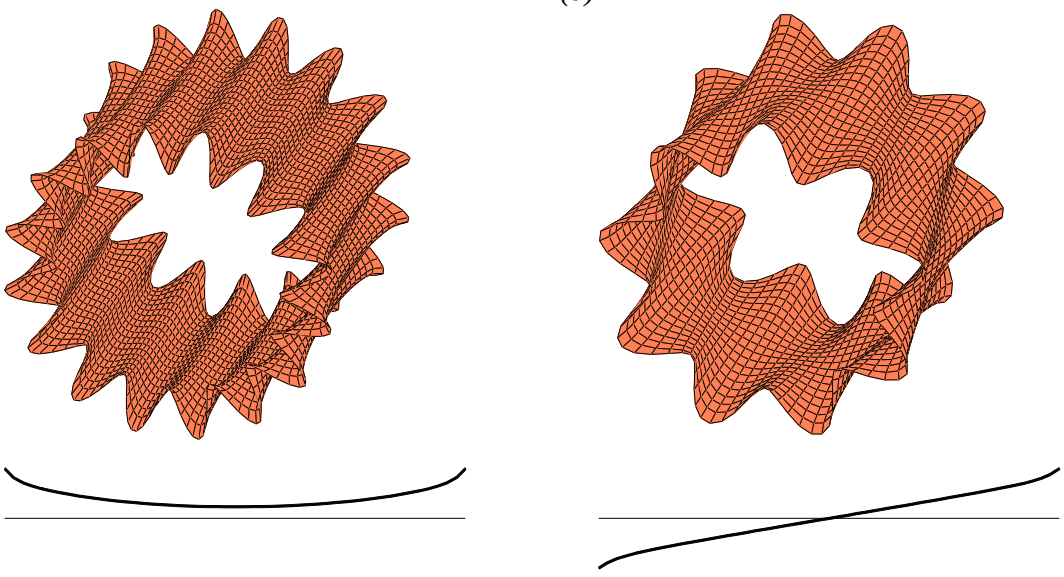

Figure 3: (a) A Rayleigh bending mode, m=-1, n=16, f=1437.5 Hz. (b)a Love mode, m=0, n=9, f=455.1Hz. Root type is 3; $\pm\alpha_1, \pm\alpha_2, \pm(p \pm \mathrm{i}q)$.

In *Figure 2* the modes (at integer circumferential numbers *n*) are highlighted using markers of different types corresponding to different types of the roots (Table 1) governing the mode shapes. For which marker type corresponds to which root type see the caption to *Figure 2*. It can be seen that indeed a large group of mode shapes are determined by the roots of type 1 (two real, two imaginary, four complex) as shown by the blue × symbols. However, the Rayleigh and Love modes are never governed by that root type. Instead, they appear to be determined by the roots of type 2, 3 and 4. Also the modes with low circumferential mode numbers (those with *n*=0 and *n*=1) are governed by roots of type 6, 7 and 8. Then also a large group of modes is determined by the roots of type 5 at higher axial

mode numbers *m* (see the right hand side of *Figure 2*). Thus it is certainly necessary to consider all eight root types in order to get all possible modes and resonance frequencies. In the right hand side of *Figure 2* it is possible to note that additional branches occur, having a steeper slope with respect to the horizontal axis, which in fact cross the branches containing the resonance frequencies of bending modes. These contain additional resonance frequencies that correspond to the longitudinal mode shapes having a pronounced axial, "in plane" deformations of the shell [7].

A comparison with an FE model of a stationary shell is given next. Two different FE meshes were used for this purpose. The first, "coarse" mesh is constituted by $x \times \phi$=40×101=5040 S4R ABACUS rectangular thin or thick doubly curved shell elements with 4-nodes, with reduced integration and finite membrane strains. The second, "fine" mesh is constituted by $x \times \phi$=40×180=7200 elements so that the number of elements along the circumference is increased by 80%. *Figure 4* shows the resonance frequencies using the same layout as in *Figure 2*, where the continuous lines are the solutions using the present exact method, and the blue circle symbols represent the resonance frequencies obtained using the FE method. It can be seen that in general the finite element analysis results fall very close to the analytical continuous lines indicating a very good agreement between the numerical and the analytical method. Some discrepancies, however, can be seen with high circumferential mode numbers of n=12 and n=13 in case the "coarse" mesh is used (left hand side of *Figure 4*). This is because such modes have 12 or 13 lobes in the circumferential direction or about 8 finite elements per wavelength so that the resonance frequencies can become overestimated by the FE method. However with the "fine" mesh having the increased number of elements in the circumferential direction the ratio goes up to 15 elements per wavelength so the resonance frequencies become more accurately calculated by the FE method. Thus the blue circles in the right hand side plot of *Figure 4* fall onto the black continuous lines almost perfectly.

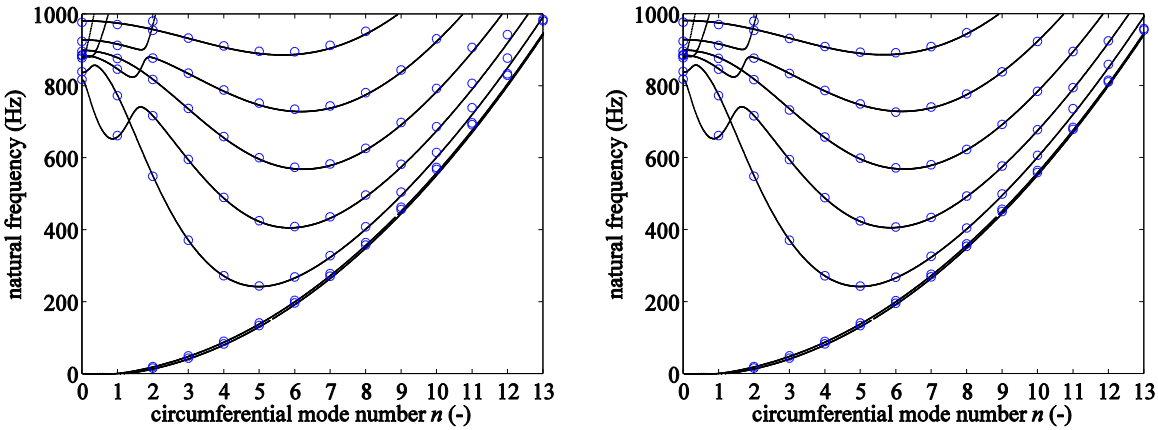

Figure 4: The comparison of natural frequencies of a stationary shell with a FE model in the range 0-1000 Hz; "rough" FE mesh (left) and a "fine" mesh (right)

Thus the present method can be considered to agree very well with the FE method and its validity is confirmed for the stationary (non-rotating) case. The validation of the present method for the rotating case is considered next. *Figure 5* follows the same layout as *Figure 4*, where the blue circles are the FE results and the black continuous lines are the exact results. The "fine" mesh is used in both plots, however the left hand side plot is for the constant rotation speed of 100 rad/s, whereas the right hand side is for the constant rotation speed of 200 rad/s around the *x*- axis. An excellent agreement between the FEM results and the analytical results can be seen so the present method is valid also for the rotating case. Note that the branches are no longer symmetric. In other words, the natural frequencies of the forward rotating modes (in the direction of rotation of the shell) are now different from their backward rotating counterparts. Thus they now rotate in opposite directions at different speeds (see Eqs. (12)-(14)).

4 CONCLUSIONS

A simplified model of a rotating tire is developed. Effects of the flexible support in the radial and circumferential direction, the initial hoop stresses due to a possible pressurisation and/or centrifugal

forces are considered in the model. The model is based on the rotating cylindrical shell having free boundary conditions. Exact expressions are given to calculate its resonance frequencies and mode shapes. An excellent agreement between the resonance frequencies obtained using the FE method and the present method is demonstrated for both stationary and rotating shells. It should be noted that the model presented relies heavily on the assumption that the air and sidewall stiffness can be approximated using an elastic foundation beneath the shell surface, which has distributed radial and circumferential stiffnesses. Also the expressions for mode shapes and the resonance frequency determinants are rather complicated. As a future work an approximate Rayleigh-Ritz methodology will be used to derive simpler expressions for natural frequencies via approximate mode shapes.

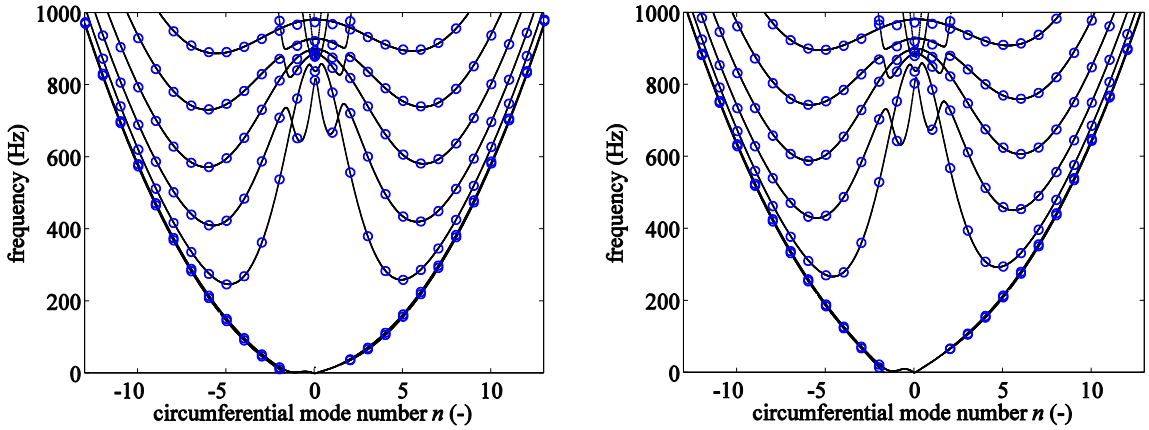

Figure 5: The comparison of natural frequencies of shell rotating with a constant speed of 100 rad/s (left and 200 rad/s (right) with a FE model in the range 0-1000 Hz using the "fine" FE mesh.

ACKNOWLEDGEMENTS

This work benefits from the Belgian Programme on Interuniversity Attraction Poles, initiated by the Belgian Federal Science Policy Office (DYSCO). Also, the Research Fund KU Leuven is gratefully acknowledged for its support. Finally, the authors acknowledge the financial support from IWT Flanders within the MODRIO project.

REFERENCES

[1] P.Kindt, P.Sas, W.Desmet: *Measurement and analysis of rolling tire vibrations*, Optics and Lasers in Engineering 47 (2009) 443–453

[2] Y.-J. Kim, J.S. Bolton: *Effects of rotation on the dynamics of a circular cylindrical shell with application to tire vibration*, Journal of Sound and Vibration 275, (2004) 605–621

[3] C. González Díaz, S. Vercammen, J. Middelberg, P. Kindt, C. Thiry, J. Leyssens, *Numerical prediction of the dynamic behaviour of rolling tyres*, Proceedings of international conference on noise and vibration engineering (ISMA), (2012.) (paper no. 890).

[4] S.C. Huang, W. Soedel, *On the forced vibration of simply supported rotating cylindrical shells*, J. Acoust. Soc. Am. 84 (1), (1988), 275-285

[5] L.R. Molisani, R.A. Burdisso, D. Tsihlas, *A coupled tire structure/acoustic cavity model*, International Journal of Solids and Structures 40 (2003) 5125–5138

[6] G. Herrmann. A . E. Armenakas, *Dynamic Behavior of Cylindrical Shells under Initial Stress*, Proc. 4th U.S. Nat. Congr. Appl. Mech. ASME, 203-213 (1962).

[7] N. Alujević, N. Campillo-Davo, P. Kindt, W. Desmet, B. Pluymers, S. Vercammen, *An analysis of free vibrations of rotating cylindrical shells having both ends free using Flügge's method*, KU Leuven, Tech. Rept. August 2014.

[8] G. B. Warburton, *Vibration of thin cylindrical shells*, Journal Mechanical Engineering Science, Vol. 7, No. 4, (1965)

[9] G. R. Kirchhoff, *Über das Gleichgewicht und die Bewegung einer elastischen Scheibe. (On the equilibrium and motion of an elastic disc)*, (1850), J. Math. (Crelle) 40.

[10] W. Soedel, *Vibrations of Shells and Plates*, 3rd edition, revised and expanded, (2004), Marcel Dekker Inc., NewYork.